JTTEE5 8:263-272

Characterization of Plasma-Sprayed Coatings Using Nondestructive Evaluation Techniques: Round-Robin Test Results*

L. Fabbri and M. Oksanen (Editors)

A round-robin test was implemented where nine European research institutions and universities applied different thermal, ultrasonic, and magnetic methods for measuring the thickness of plasma-sprayed coatings. The coatings, which had thicknesses ranging from 50 to 500 μm, were applied on substrates of AISI 316, a standard industrial structural material, and on Armco iron in order to have a material of known thermal properties. Destructive testing was performed after the other methods had been applied, resulting in detailed information on the coating thickness, rugosity, and uniformity. The results obtained with the applied methods on the two unknown samples for each substrate type agreed within 20% with the destructive testing data.

Keywords defect sizing, photothermal, plasma-sprayed coatings, round-robin test, thermal diffusivity, thickness

1. Introduction

Plasma-sprayed coatings are widely used for many industrial applications to protect gas turbine hot section components from surface degradation. Nevertheless, the use of the coatings in advanced technologies is hampered by the lack of accepted standards and norms for their qualification and testing. For several years, the Institute for Advanced Materials (IAM) of the Joint Research Centre of the European Commission (JRC) has worked to trigger the development of methods and procedures for the characterization of coatings to ease their industrial use. For the JRC, being a Pan-European research organization, this type of European normative research is by definition one of the institutional goals.

As a first step, the I Workshop on Characterization of Coatings by NDE Techniques was organized (13-14 Dec 1993, JRC Ispra, Italy) where the importance of the development of standardization procedures was widely recognized. To start the process for identification and improvement of characterization methods for coatings, and to define norms and standards, it was decided that the first attempt should be at comparing the results of different methods for thickness measurements and defect sizing that are presently being developed on a laboratory scale. A round-robin test was defined in which a small number of specimens were circulated among the laboratories. This joint project included nine European institutions (six universities, two industrial research centers, and the JRC) from five different countries. The funding for this project was supplied by each of the participating laboratories.

The task of individual partners consisted of the determination of coating thicknesses and the location of artificial defects in selected specimens. The results obtained in the different laboratories were collected by IAM for discussion with all participants. In this framework, the II Workshop on the Characterization of Coatings by NDE Techniques was organized at the JRC Ispra, Italy, on 22-23 Feb 1996.

One of the goals of this exercise was a presentation of the results to possible interested industries and then to install a common program for further development of characterization methods and procedures for industrial applications. This should be considered as a first step in the elaboration of other activities of general interest such as the assessment of coating life time, process monitoring during production, and the repair and recycling of coating components.

2. Round-Robin Test: Nondestructive Methods

Most of the experimental methods used in this round-robin exercise for coating thickness, L, and thermal diffusivity, α, evaluation are based on the photothermal effect, that is, the generation of thermal waves by intensity modulated or pulsed optical excitation (Ref 1, 2). In other words, these techniques probe material properties through the detection of temperature distribution induced by external heating. Photothermal methods are generally nondestructive, contactless, and single sided, and therefore offer great potential in the area of nondestructive evaluation (NDE). This has already resulted in the construction of commercially available instrumentation for several applications of technological interest. For coating systems, the propagation of heat is affected by the presence of a thermal mismatch at the coating-substrate interface. When pulsed excitation is used, this effect is reflected in the time evolution of the surface temperature, whereas for periodical heating, the thermal mismatch modifies the propagation properties of the thermal waves. In both cases, the analysis of the coating surface temperature gives information on coating properties through an inversion

*This article was first published in INSIGHT—Non-Destructive Testing and Condition Monitoring, *The Journal of The British Institute of Non-Destructive Testing*, Vol 39 (No. 12), Dec1997, and appears here with the permission of The British Institute of Non-Destructive Testing and the authors. This article was composed by the working group; see Acknowledgment.

L. Fabbri, JRC Institute for Advanced Materials, PO Box 2, 1755 ZG Petten, The Netherlands; and **M. Oksanen,** Nokia Research Center, P.O. Box 407, FIN-00045 Nokia Group, Finland. Contact M. Oksanen at e-mail: Markku.A.Oksanen@research.nokia.com.

procedure. A point to note is that the thermal perturbations only reach a limited depth in the material, which can be varied by changing the observation time (pulsed regime) or the frequency range of the heating source (periodic regime). In the framework of the round-robin exercise, both periodic and pulsed techniques were employed. Despite the different methods of detecting the temperature field, all the techniques used by the participants can be classified as belonging to the two methods described in the following paragraphs: thermal wave interferometry (TWI) and pulsed photothermal radiometry (PPTR).

Thermal wave interferometry (Ref 3-8) is based on the propagation of a plane thermal wave through a two-layer structure (e.g., a coating on a substrate). The thermal wave is produced on the coating surface by a broad heating source that is temporally modulated at an angular frequency $\omega = 2\pi f$ (periodic regime), and the wave then propagates to the coating-substrate interface, at which it is partially reflected. Due to the coherence of primary and reflected waves, interference phenomena will occur, resulting in a modification of the surface temperature, which is related to subsurface features. For a coating with thickness L, thermal diffusivity, α, and conductivity, k, the harmonic component of the temperature rise induced by a broad optical heating of intensity, I_o, can be expressed as follows (Ref 3):

$$T_{ac} = \frac{I_o\beta}{2\sigma k[1 - \Gamma \exp(-2\sigma L)]}\left[\frac{1 - \exp[-(\beta + \sigma)L]}{\beta + \sigma} + \Gamma \exp(-2\sigma L)\frac{1 - \exp[-(\beta - \sigma)L]}{\beta - \sigma}\right] \quad \text{(Eq 1)}$$

where β is the coating optical absorption coefficient, and σ the complex thermal wave number defined as $\sigma = (1 + i)[\omega/(2\alpha)]^{1/2}$. The thermal wave reflection coefficient, Γ, depends upon the thermal effusivity ratio, b, of the substrate-coating system:

$$\Gamma = \frac{1 - b}{1 + b} \quad \text{(Eq 2)}$$

where $b = e_s/e_c = c\sqrt{\alpha_s/\alpha}$ (c is the substrate-coating volumetric heat capacity ratio and α_s is the substrate thermal diffusivity).

Pulsed photothermal radiometry (Ref 9-11) consists of heating part of the coating with a short duration heat pulse and monitoring the temperature decay as a function of time as the heat diffuses into the sample (impulse regime). For a Dirac pulse, the analytical expression for the decay of the normalized temperature at the surface of an opaque ($\beta = \infty$) two layer sample is (Ref 12):

$$T = \frac{I_o\beta}{\sqrt{\pi\, te_c}}\int_0^L \exp(-\beta\xi)\left[\exp\left(-\frac{\xi^2}{4\alpha_c t}\right) + \sum_{n=1}^{\infty}\Gamma^n\left[\exp\left(-\frac{(2nL - \xi)^2}{4\alpha_c t}\right) + \exp\left(-\frac{(2nL + \xi)^2}{4\alpha_c t}\right)\right]\right]d\xi \quad \text{(Eq 3)}$$

where all the parameters are defined as above. When the thermal effusivity of the coating and the substrate are the same, the surface temperature continues to decay as $t^{-1/2}$. By contrast, when the thermal effusivity of the substrate is less than the coating, heat propagation into the substrate is impeded, and the surface temperature shows a decrease in the rate of decay. If the thermal effusivity is higher than the coating, heat flows more quickly into the substrate, and the surface temperature decreases more rapidly.

For both methods, the temperature dependence on frequency (or time) is completely defined by assigning proper values for Γ, β, and the L^2/α ratio. However, the thermal reflection coefficient, Γ, and the L^2/α ratio are not completely independent parameters. If the thermal properties of the substrate and the volumetric heat capacity ratio are known, the temperature frequency (or time) dependence is completely described by β and the L^2/α ratio. These quantities can be obtained from the experimental curves through data reduction based on an inversion procedure. The determination of the L^2/αratio can be used to determine the thermal diffusivity of the coating if the thickness is known, or vice versa.

Many methods for detecting the surface temperature were used by the different participants. Infrared radiometry (IR) (Ref 13-15) was by far the most widely used method in this round-robin test. This detection technique is based on measuring the thermal wave field at the coating surface by detecting the emitted thermal radiation. Infrared radiometry offers the advantage that the sample sizes and shapes are not restricted. Besides, the detection geometry is very flexible, varying from point to wide-field detection.

Radiometric detection can also be realized using scanning and matrix area cameras (video thermography, or VT). Each pixel of the image camera is equivalent to a local radiometric measurement. In this case, the main problem consists of the signal treatment due to the fast and large flow of data. Conventionally, NDE cameras are used along with pulsed excitation (i.e., observation of single images as functions of time after a short illumination of the sample surface), but more recently results have been obtained with modulated excitation and lock-in detection of periodic surface temperatures (lock-in thermography, or LT) (Ref 16-17). This version of multiplex photothermal radiometry allows for quick phase angle images of large areas at low frequencies.

The last two detection methods used in the present exercise were the mirage (M) and photoacoustic (PA) techniques. In the first technique, a continuous wave laser beam was used to probe the surface temperature through the measurement of the refractive index gradient in an air layer close to the sample surface (Ref 18-20). In a photoacoustic gas cell, the thermal wave on the sample was detected through observing the propagation of the thermally generated acoustic waves that propagate into the fluid above the sample surface. This detection system is also available as a supplement to commercially available equipment (thermal wave microscope ALADIN (Ref 21) that was employed by one of the participants in the round-robin test.

Besides photothermal methods, eddy current and high-frequency ultrasonic techniques were used. The eddy current method is based on the impedance change of a current-carrying coil that is used to induce an eddy current in conducting materials, which in turn opposes the alternating magnetic field (Ref 22). In ultrasonic methods the phase velocity and attenuation of the ultrasonic wave are correlated with the coating properties. Unfortunately only one of the four laboratories that also used ultrasonic methods supplied coating thickness data.

3. Sample Selection

Due to the nonavailability of reference specimens that could be used as certified standards for the coating thickness evaluation and defect sizing, a set of samples was prepared at the Joint Research Centre on a laboratory scale. Yttria partially stabilized zirconia (YPSZ) was selected as the coating material due to its large employment for industrial applications. Its popularity is due to its very low thermal conductivity, its low variation in conductivity as a function of temperature, its high coefficient of thermal expansion ($10^{-5}K^{-1}$), which reduces the thermal expansion difference between the coating and metal substrates, and its good electrical insulation (Ref 23-25).

The coating was deposited by plasma spraying carried out in an open atmosphere using a Plasma Technik F4 MB 92021 gun (Plasma Technik AG, Wohlen, Switzerland), and the set of spray parameters specified in Table 1. These parameters were fixed in order to obtain a similar level of porosity among the different samples.

The commercial powders (Metco-204NS, Westbury, USA) consisted of 8 wt% Y_2O_3 partially stabilized ZrO_2 with typical sizes in the 10 to 100 μm range (stabilized in the tetragonal phase with a small amount in the monoclinic phase).

A first set of samples was prepared by using Armco iron (Armco Steel Corporation, Middletown, Ohio) as the substrate material. Armco iron has no specific industrial interest as a coating substrate. Nevertheless it is currently used as a standard for thermal diffusivity measurements, and it is therefore very useful when thermal wave techniques are involved (Ref 26, 27). In a second set of samples, the YPSZ coatings were deposited onto a stainless steel substrate (AISI 316) with a NiCoCrAlY bond coat in between (AMDRY 995, 37.93 wt% Co, 32.5 wt% Ni, 21.9 wt% Cr, 8.41 wt% Al, 0.05 wt% O_2, and 0.02 wt% C). Although in this case the description of thermal wave propagation is more complicated, the selection of these materials and the choice of a three-layer configuration are much closer to practical industrial needs. This justifies the use of the present set of samples in the round-robin exercise.

The three different samples that were produced for each coating-substrate combination had a flat geometry (125 by 20 by 5 mm and 120 by 20 by 5 mm for the Armco iron and AISI 316, respectively) and included more thickness steps with different coating thickness (Fig. 1). Specifically, for each series, the following samples were available: (a) two calibration strips with three steps of known thickness and (b) one strip with two steps of unknown thickness.

The multistep structure was produced with further plasma-sprayed depositions after masking the selected surface of the coating.

An attempt to produce bonding defects was made on yet another strip of YPSZ coated on AISI 316, which had a bond coating in between that was submitted to laser treatment before deposition of the YPSZ coating. A 5 kW CO_2 laser with a beam diameter of approximately 8 mm was used, and the treatment consisted of five 80 ms pulses in the same area. This procedure was performed at two different positions located approximately at the center of the selected strip. After, a homogeneous coating of YPSZ (~400 μm thick) was deposited using the procedure described above.

For all the calibration specimens, the coating thickness was determined at the center of each step by measuring the difference in the thickness of the specimen before and after coating deposition (micrometer thickness) (Ref 28). Specifically, the measuring position was carefully recorded before deposition but after sanding and cleaning of the substrate surface. Then the thickness was measured using a machinist's micrometer accurate to 10 μm. After the deposition, the surface was cleaned of superficial powder and the measurement was repeated at the same location. All the measurements were carried out by taking at least five readings for each position. Table 2 reports the results. An uncertainty of ±20 μm was estimated. All the data on AISI 316 substrate samples (strips 3 and 4) include the AMDRY 995 bond coat, hence the thickness values in Table 2 are the sum of the ceramic coating and the bond coating.

4. Round-Robin Test: Destructive Analysis

After the round-robin exercise, all the samples were collected at the JRC for destructive evaluation. Each strip was cut perpendicularly to its length and approximately at the center of each step using a low-speed diamond saw. The cross sections were used for the evaluation of coating thickness by optical

Table 1 Plasma spraying conditions for the 8 wt% Y_2O_3 ZrO_2 coatings

Arc power, kW	35
Flow rates, L/min	Ar (primary): 30 H (secondary): 5 Ar (carrier): 3.2
Transverse gun speed, m/s	0.1
Spray distance, mm	125
Atmosphere	Open air
Substrate temperature, °C	140

Table 2 Analysis of coating micrometer thickness for calibration specimens

Strip No.	Substrate	Bond coat	A, μm	B, μm	C, μm
1	Armco	None	70	120	150
2	Armco	None	180	230	280
3	AISI 316	AMDRY 995	270	320	390
4	AISI 316	AMDRY 995	430	500	540

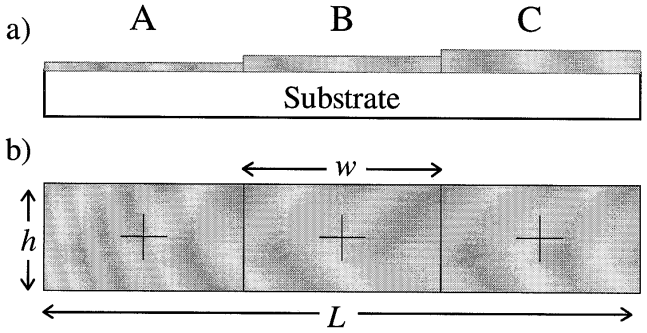

Fig. 1 Three-step calibration strip with different coating thicknesses. (a) Cross section. (b) View from the top. h = 30 mm, w = 40 to 42 mm, L = 125 mm for Armco substrate, L = 120 mm for AISI 316 substrate

means. Due to the surface roughness typical of plasma-sprayed coatings, the actual thickness is not clearly defined. However, the use of plane thermal waves as the testing tool suggests a definition of the thickness based on the average distance between the two coating profiles (i.e., surface and interface).

Specifically, the coating roughness profiles, taken from cross-sectional micrographs, were reproduced on transfer paper, digitized, and lines were fitted to the profile, as described in detail elsewhere (Ref 29). The average distance between the two lines, not necessarily parallel, obtained by fitting a line to the coating profile was taken as the coating thickness. Furthermore, by collecting the single profiles coordinates, that is, the n points (x_i, y_i) using the fitted lines as the reference system for each profile, it was possible to determine the roughness, R_a:

$$R_a = \frac{1}{n}\sum_{i=1}^{n} |y_i|$$

the standard deviation of the coating profiles:

$$\sigma_{n-1} = \sqrt{\frac{1}{n-1}\sum_{i=1}^{n} y_i^2}$$

and the correlation length defined as the width of the highest peak of the autocorrelation function R_{xx} at –3 dB from its maximum:

Table 3 Destructive analysis on YPSZ Armco calibration samples for specimens 1 and 2

	YPSZ Armco 1			YPSZ Armco 2		
Calibration samples	**A**	**B**	**C**	**A**	**B**	**C**
Top						
R_a, μm	9	11	8	9	13	12
σ_{n-1}, μm	11	13	10	12	17	15
Corresponding length, μm	76	135	52	67	144	77
Interface						
R_a, μm	5	5	5	4	4	5
σ_{n-1}, μm	6	5	6	7	5	6
Corresponding length, μm	22	19	34	27	17	24
Geometry						
L, μm	**72 ± 25**	**108 ± 27**	**174 ± 23**	**161 ± 27**	**233 ± 35**	**272 ± 32**
Angle, degrees	0.07	0.1	0.8	0.7	0.05	1.3
$\lvert\Delta L/L\rvert$, %	3	11	14	11	0.4	3

Table 4 Destructive analysis on YPSZ AISI 316 calibration samples for specimens 3 and 4

	YPSZ AISI 316 3			YPSZ AISI 316 4		
Calibration samples	**A**	**B**	**C**	**A**	**B**	**C**
Top						
R_a, μm	9	9	9	6	12	12
σ_{n-1}, μm	11	11	12	8	15	16
Corresponding length, μm	53	60	69	78	137	74
Interface (bond coating)						
R_a, μm	5	6	6	5	6	5
σ_{n-1}, μm	6	8	7	6	7	6
Corresponding length, μm	39	62	85	55	53	41
Interface (substrate)						
R_a, μm	4	5	4	5	5	4
σ_{n-1}, μm	6	6	5	6	6	5
Corresponding length, μm	22	26	17	67	42	30
YPSZ						
L, μm	112 ± 25	179 ± 27	220 ± 27	314 ± 20	379 ± 32	389 ± 32
Angle, degrees	0.01	1.3	0.01	0.5	1.5	1.6
AMDRY 995						
L, μm	131 ± 17	145 ± 20	149 ± 17	115 ± 17	124 ± 18	115 ± 15
Angle, degrees	0.2	0.3	0.31	0.4	0.4	0.8
L, μm, **total**	**243 ± 30**	**324 ± 34**	**369 ± 32**	**429 ± 26**	**503 ± 37**	**504 ± 35**
$\lvert\Delta L/L\rvert$, %	11	1	6	0.2	0.6	7

$$R_{xxj} = \sum_{k=0}^{n-1} x_k x_{j+k} \quad j = -(n-1), \ldots, -1, 0, 1, \ldots, (n-1)$$

These parameters were calculated for each profile of the coating (i.e., the top and the substrate interface) at a spatial distance of 1 mm.

Tables 3 and 4 report the data obtained on all the calibration specimens (i.e., strips 1 to 4) where, as in Table 2, the letters A, B, and C refer to the different thickness steps. As expected, the roughness, and hence the coating standard deviation, is much higher at the top of the coating than at the coating substrate and the coating-bond coat interfaces. The angles between the two fitted lines of the coating profiles were also calculated. They give information about the systematic variation of the coating thickness in the selected section. For example, the 1.3° angle of the C step of strip 2 (YPSZ-Armco) corresponds to a thickness variation of approximately 23 μm in a cross section 1 mm long. A point to note is that for the AISI 316 substrate specimens (strips 3 and 4), the coating thickness included the bond coat.

The thickness data are reported together with their uncertainties that represent the semiamplitude of the thickness interval, corresponding to a 95% probability in the *t*-student distribution. Despite the large roughness values, the uncertainties are quite limited, ranging between 10 and 30% for YPSZ-Armco and 5 and 10% for YPSZ AISI 316. A comparison with the micrometer thickness data in Table 2 exhibits a relative variation, $\Delta L/L$, that is always under 15%. This result is rather acceptable if the slight difference in the definition of average thickness and micrometer thickness is considered, which refers to the distance between the top surface highest peaks and the mean line of the interface. In addition, the accuracy of the micrometer method was quite limited (±20 μm) and accounts for large relative errors when measuring thin coatings.

For the two specimens with unknown thicknesses, hereafter named the unknown samples, and consisting of two-step strips (A and B, respectively) the same destructive analysis was performed. Tables 5 and 6 show the results.

From Tables 4 and 6, it should be recognized that although the AMDRY 995 bond coats were deposited using the same processing parameters for the different strips, their thicknesses were quite different, ranging between 120 and 140 μm (average values within the same strip).

Table 5 Destructive analysis on the two step YPSZ Armco sample with unknown thickness

	YPSZ Armco	
Unknown sample	**A**	**B**
Top		
R_a, μm	10	9
σ_{n-1}, μm	14	11
Corresponding length, μm	103	72
Interface		
R_a, μm	4	4
σ_{n-1}, μm	6	5
Corresponding length, μm	26	17
Geometry		
***L*, μm**	**73 ± 30**	**118 ± 24**
Angle, degrees	0.6	0.36

Table 6 Destructive analysis results on the two step YPSZ AISI 316 sample with unknown thickness

	YPSZ AISI 316	
Unknown sample	**A**	**B**
Top		
R_a, μm	7	10
σ_{n-1}, μm	10	12
Corresponding length, μm	69	59
Interface (bond coating)		
R_a, μm	6	5
σ_{n-1}, μm	7	5
Corresponding length, μm	155	51
Interface (substrate)		
R_a, μm	4	4
σ_{n-1}, μm	5	5
Corresponding length, μm	104	33
YPSZ		
L, μm	169 ± 24	250 ± 25
Angle, degrees	0.3	0.16
AMDRY 995		
L, μm	120 ± 17	122 ± 14
Angle, degrees	0.09	0.17
***L*, μm, total**	**289 ± 30**	347 **± 30**

5. Round-Robin Test: Nondestructive Analysis

The thickness measurements of the unknown samples were performed by all the participants with a variety of apparatuses and procedures as compiled in Table 7. All values were measured as close to the center of each different thickness "step" as possible.

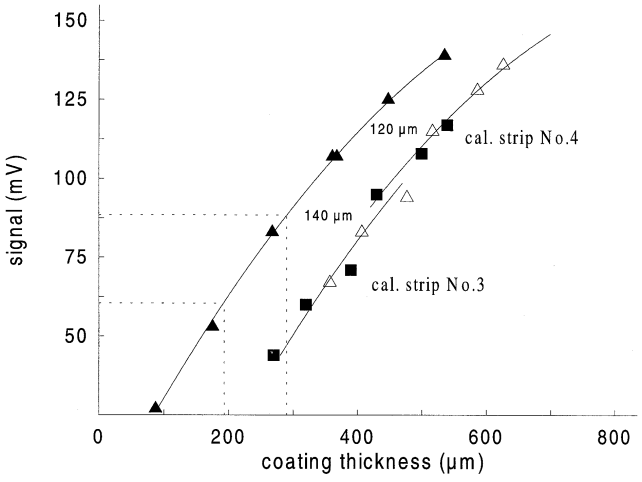

Fig. 2 Eddy current measurement on YPSZ-AISI 316 samples. σ calibration data with plastic sheets on the substrate. ν data on the different coating steps (strips 3 and 4). Δ data on coating steps plus plastic sheets (by participant 7)

5.1 Eddy Current Methods

The data obtained using eddy currents (participants No. 6 and 7) agrees to within 7% for all coatings. For the Armco substrate samples, the measurement was performed using a magnetic thickness gauge (participant 6) or by saturating the magnetic field, in order to reduce hysteresis effects, and using the eddy current probe (participant 7). For the AISI 316 substrate specimen, the data refer to the ceramic coating alone because the eddy current probes were calibrated using only plastic sheets and not the calibrated samples. As all the other data of the round-robin test include the thickness of the bond coat, the eddy current data were transformed by adding bond coat thickness measured during the destructive session (Table 6). The transformed values are shown second.

The analysis of eddy current measurements on calibration specimens gives information on the thickness of the bond coat. This is shown in Fig. 2 where the eddy current signal is plotted versus thickness. Specifically, the measurements on the different steps of the calibration specimens (filled squares) were compared to those obtained using plastic sheets placed directly upon the substrate (solid triangles). In order to increase the number of points, plastic sheets were also employed on the calibration specimens (empty triangles). By measuring the shift of the data from the calibration curve, bond coat thickness values of 140 ± 20 μm and 120 ± 10 μm were obtained for steps 3 and 4, respectively. The uncertainties were assessed from the scattering of measuring points and the shifted calibration curve. These data are in a very good agreement with those obtained with destructive testing: 142 and 118 μm, respectively (average from Table 4).

A point to note is that eddy currents are sensitive to the distance between the highest peaks of the coating surface and the mean line of the interface. Due to roughness, this distance differs from the definition of coating thickness given in section 4. Hence, in general eddy current data should be added to the distance of the highest peak from the top surface mean line, to be compared to the destructive test data (Tables 5 and 6). For the Armco specimen, the eddy current data are very close to those obtained after destructive testing. This conjunction is rather surprising and has no evident explanation. On the contrary, data obtained on the AISI 316 substrate specimen are smaller than the values measured after destructive testing by approximately 20 and 60 μm (step A and step B, respectively).

5.2 Photothermal Techniques

Thickness measurements using photothermal techniques were performed by all the round-robin participants (Table 7). Eight samples of independent data were obtained using thermal wave interferometry with different equipment and temperature detection systems: infrared radiometry (participants 1, 3, 4, 5, and 7), infrared lock-in thermography (participant 1), ALADIN P1 in combination with the photoacoustic cell (participant 2), and mirage detection (participant 9). Three samples of data were obtained by pulsed photothermal radiometry with both video thermography (participants 2 and 8) and infrared radiometry (participant 6). Table 8 summarizes experimental conditions used by the different participants (that is, heating parameters, temperature detection system, and frequency or time range). The general relationship between the coating thickness and the photothermal signal was assessed by all the participants using the calibration samples. An analysis of the photothermal signal for the periodical and pulsed techniques was performed in the frequency and time domain, respectively.

With regard to the data reduction methods, some participants obtained the calibration curves by interpolating the data of the photothermal signal versus the reference thickness for certain values of the modulation frequency (or the time). As an example, Fig. 3 shows the calibration curves obtained using thermal wave interferometry IR (participant 1) at two different frequencies (0.5 and 1 Hz). Here the phase signal measured from YPSZ-AISI 316 calibration specimens is plotted as a function of the micrometer thickness value that was supplied with the samples.

Table 7 Round robin test: thickness results

Method	YPSZ Armco A	YPSZ Armco B	YPSZ AISI 316 A	YPSZ AISI 316 B	Participant No.
EC	70 ± 25	120 ± 25	195 ± 10(a) (315)	290 ± 10(a) (412)	7
EC			199 ± 6(a) (319)	289 ± 8(a) (411)	6
EC (MTG)	75 ± 4	121 ± 6			6
TWI (IR)	90 ± 10	130 ± 10	370 ± 11	430 ± 7	1
TWI (ILT)	…	180 ± 20	315 ± 20	350 ± 20(b)	1
TWI (PA)	80 ± 20	100 ± 20	320 ± 20	390 ± 20	2
TWI (IR)	67 ± 1	121 ± 2	338 ± 17	418 ± 12	3
TWI (IR)	100 ± 30(b)	250 ± 100(b)	400 ± 100(b)	500 ± 100(b)	4
TWI (IR)	70 ± 3	125 ± 10	340 ± 5	407 ± 3	5
TWI (IR)	77 ± 8(c)	118 ± 12(c)	325 ± 10	430 ± 15	7
	83 ± 9(c)	119 ± 13(c)			7
TWI (M)	45 ± 7(b)	55 ± 7(b)	…	…	9
PPTR (IR)	70 ± 9	134 ± 23	340 ± 43	415 ± 40	6
PPTR (VT)	70 ±	120 ±	320 ±	390 ±	8
PPTR (VT)	100 ± 50(b)	200 ± 50(b)	250 ± 50(b)	400 ± 50	2
US	70 ± 20	100 ± 20	310 ± 20	390 ± 30	2

ED, eddy current; MTG, magnetic thickness gauge; TWI, thermal wave interferometry; IR, infrared radiometry; M, mirage; ILT, infrared lock-in thermography; PA, photoacoustic; OBD, optical beam deflection; PPTR, pulsed photothermal radiometry; VT, video thermography; US, high-frequency ultrasound. (a) Does not include the bond coat thickness. (b) Data refer to results that are outside the general trend for reasons explained in the text. (c) Same data but different data reduction

The measurements on unknown samples together with the calibration curves can be used to obtain their coating thickness (cross points in Fig. 3).

A different approach was used by other participants. This consisted of the analysis of the frequency (or time) dependence of the photothermal signal. Specifically, because a photothermal signal depends upon the L^2/α ratio, by determining the average value of thermal diffusivity of YPSZ from the calibration specimens, the thickness of the unknown samples can be obtained by fitting the theoretical model to the experimental data. This method requires the validity of several assumptions such as knowledge of the frequency dependence of detection system, absence of heat loss, uniform heating, presence of a perfect two-layer system, etc. Thus it cannot be applied at all times.

The case of samples having Armco iron as the substrate is particularly favorable because the thermal properties of this material are well known and quite similar from batch to batch. This means that the frequency (or time) dependence of the photothermal signal depends almost exclusively upon the L^2/α ratio and the absorption coefficient β (the densities of two materials are known, and their specific heats are structure-independent properties, hence literature values could be used) (Ref 30). Measurements on the unknown samples having Armco iron as the substrate, which were performed using thermal wave interferometry IR, are shown in Fig. 4 (participant 7). The solid lines were calculated by a least-square procedure having L and β as the fitting parameters and a fixed value of $\alpha = 0.0057 \times 10^{-4}$ m^2/s, as measured from the calibration specimens. The results on thickness were 77 and 118 μm, as shown in Table 7. For a comparison, the same set of measurements was submitted to a data reduction method based on three calibration curves: 6, 7, and 8 Hz, respectively. The values for the thinner coating agreed to within 7.5%, whereas for the thicker coating a better result was achieved (<1%).

5.3 Ultrasonic Method

The last data in Table 7 were obtained using a high-frequency, ultrasonic pulse-echo technique. A focused 50 MHz transducer was used to produce longitudinal waves at normal incidence with a spike pulse excitation mode, and the echo detection was realized using a 400 MHz transient digitizer. A separation of surface and interface echoes and simple time-of-flight measurement is impractical due to the coating roughness. However, the study of time-of-flight of longitudinal wave in the coating and the analysis of echo width and shape gives information about the coating thickness. The influence of coating roughness was reduced through spatial averaging over the coating B-scan.

5.4 Comparison of Thickness Data

The thickness data of the round-robin test are summarized in Table 7 and Fig. 5 and 6. The results in Table 7 notated by footnote (b) represent values that deviate from the media of the others reported. Obvious reasons exist for participant 4 where a system with a lower frequency limit of 10 Hz was utilized, thus the necessary phase contrast was not obtained for coatings of this thermal thickness. Participant 9 used a measurement system, which due to mechanical limitations, could only measure the reduced coating thickness at the corners of the test piece. However this limitation is by no means representative and can be easily overcome using a more sophisticated experimental system (Ref 31). As for participant 2, the data reduction was reported to have been performed applying values of thermal properties for the bulk that can be considered representative, but are not the exact values used by others in similar calculations.

The internal scattering of the thickness data is quite small (see Fig. 6 and Table 9); however, in comparison with the thickness data obtained from destructive tests (solid lines in figures), there is an unexplainable shift up in the values reported that is particularly notable for the AISI-316 substrate samples. One possible hypothesis to explain this difference is that the bond coat that was applied to the AISI 316 substrate was not uniform from sample to sample. In addition it should be noted that with

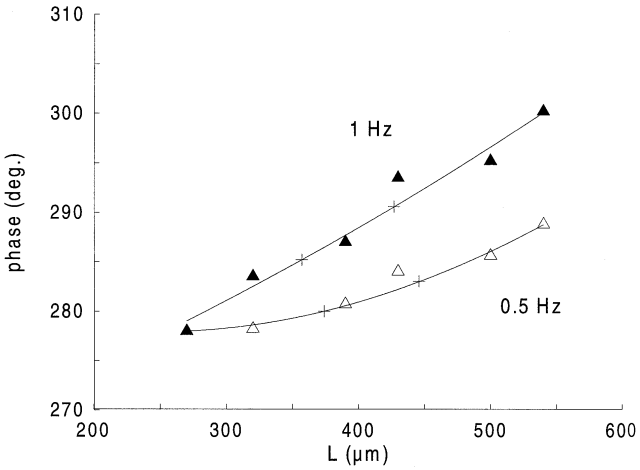

Fig. 3 Thermal wave interferometry. Calibration curves obtained on the YPSZ-AISI 316 specimens at 1 Hz (σ) and 0.5 Hz (Δ). The symbol + refers to the measurements on samples with unknown thickness (by participant 1).

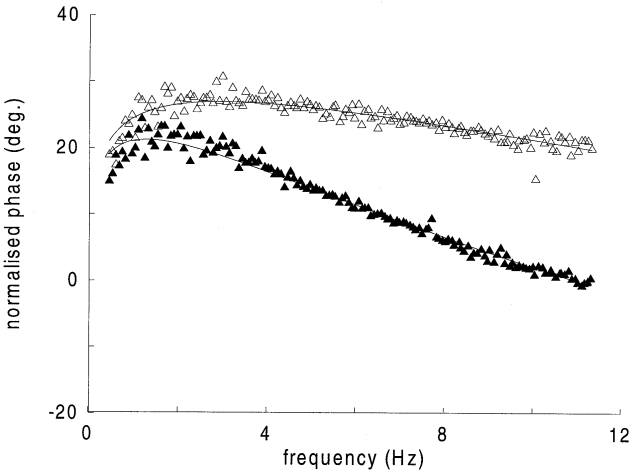

Fig. 4 Thermal wave interferometry. Normalized phase versus frequency. Measurements on YPSZ-Armco sample with unknown thickness. σ experimental data on step A. Δ experimental data on step B. The solid lines are the best fitting curves with the following parameters: $\alpha = 0.0057$ cm^2/s, $\Gamma = -0.79$, $\beta = 0.3 \times 10^4$ m^{-1}, $L = 77$ μm (σ step A), and $L = 118$ μm (Δ step B) (by participant 7)

differences of 10 to 20%, the effect of minor changes in deposition parameters, number of deposited layers (passes of the spraying gun), and so on, can modify the thermal properties of the coating. Therefore the reference and unknown samples might in effect have a different type of coating, thus rendering the calibration procedure ineffective. It can be easily shown that the difference of 15 or 18% seen in Table 9 corresponds to a thermal diffusivity change of 7.5 and 9%, respectively.

Measurements of coating thermal diffusivity were performed by six participants (Table 10). The thermal diffusivity of the plasma-sprayed zirconia coating was found to be a function of thickness; therefore average values are reported. The underlined results are considerably different from the others and are in error due to either having performed the calibration measurements at sample corners where the thickness was smaller than the calibrated value (TWI, M) or die to having underestimated the thermal diffusivity of the bulk ceramic material (TWI, M).

All the α data found for the coatings were considerably lower than the values reported by Hasselman (0.014 cm^2/s) for a monolithic material having a similar composition (8.6 wt% Y_2O_3-ZrO_2). This reduction was reported also by Brandon and Taylor (Ref 25) and Brant et al. (Ref 32) and is typical for plasma-sprayed coatings due to the high porosity and impurities.

The effects of laser heat treatment of the bond coat were not detected correctly by any of the participants; moreover different approaches showed defects in places where there should not have been any with no correlation between methods. Only small

Table 8 Experimental conditions

Participant No.	Frequency/time range	Heating sources	Detection system
1	0.5 and 1 Hz	Ar^+ laser (P = 0.4 W, a = 5 mm)	MCT
	0.06 Hz	1 kW lamp	IR camera Agema 900 Agema lock-in system
2	2 Hz-5 kHz	Nd-YAG laser (P = 0.1 W, a = 0.6 mm)	InAs and photoacoustic cell (ALADIN P1 microscope)
	1.5 s, typically	6.4 kJ flash lamp	IR camera Inframetrics 600
3	1 Hz-20 kHz	Ar^+ laser (P = 0.6 W, a = 1.25 mm)	MCT R = 0.6 mm
4	10 Hz-1 kHz	Ar^+ laser (P = 2 W, a = 5 mm)	MCT R = 50 μm
5	2 and 4 Hz	Ar^+ laser (P = 1 W, a = 1 mm)	TGS
6	1s, typically	Nd-YAG laser τ < 100 ns, (I = 50 mJ/cm^2, a = 20 mm)	InSb-MCT R = 2 mm
7	1-10 Hz	Ar^+ laser (P = 0.8 W, a = 3mm)	MCT R = 50 μm
8	1-2 s, typically	Flash lamps	IR camera Agema 880LWB
9	1 Hz-4 kHz	Ar^+ laser (P = 0.3 W, a = 3 mm)	He-Ne laser Quadrant position sensor

MCT, mercury cadmium telluride; TGS, triglycine sulphate pyrometer; P, power; E, energy; a, 1/e-gaussian radius; R, spotted area radius

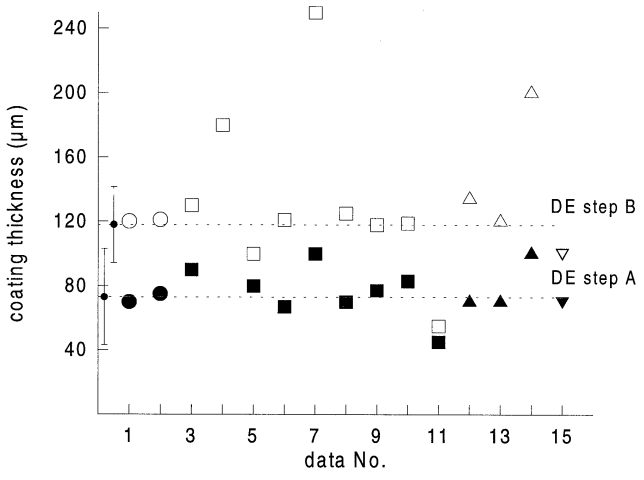

Fig. 5 Round-robin test: thickness data on YPSZ-Armco unknown samples. The black and white symbols refer to steps A and B, respectively. The closed circle datapoints are eddy current, ν is TWI, σ is PPTR, and τ is US. The dotted lines indicate the data obtained by destructive testing.

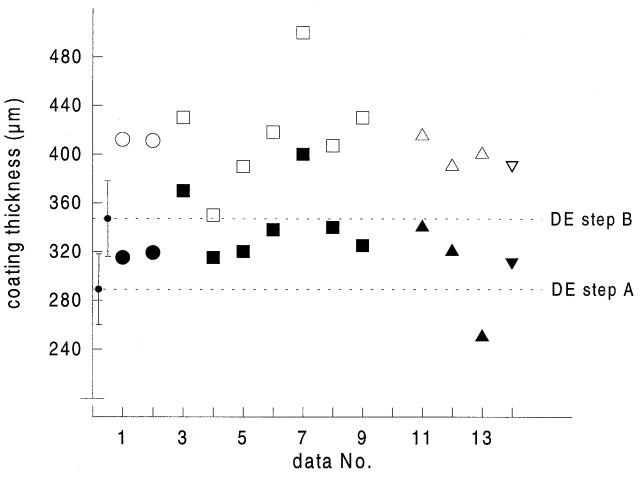

Fig. 6 Round-robin test: thickness data on YPSZ-AISI 316 unknown samples. The black and white symbols refer to steps A and B, respectively. The closed circle datapoints are eddy current, ν is TWI, σ is PPTR, and τ is US. The dotted lines indicate the data obtained by destructive testing.

cracks at the corners of the pieces were correctly identified by most participants; however, these were not deliberate defects. It turns out that the laser induced defects were too "weak" and perhaps nonrepresentative of real defects to be detected using the methods applied.

6. Conclusions

A round-robin exercise including nine participating European laboratories comparing various nondestructive methods for the determination of plasma-sprayed coatings thicknesses was implemented. The methods applied spanned most of the applicable photothermal, ultrasonic, and eddy current techniques. As a reference measurement, destructive evaluation, using advanced optical methods capable of determining the statistical indicators describing the coatings surface and interfacial structure, was used.

The results obtained for coatings deposited alone on Armco iron were in good agreement with values obtained by destructive analysis. On the other hand, the two-layer system represented by zirconia on a metallic bond coat of similar thickness caused some systematic deviation of the results from the actual thickness. This was probably due to the difference in the bond coat thickness of the calibration samples and of the unknown samples. In addition, even a slight variation in the coating thermal diffusivity could manifest as a difference in thickness values. This underlines the problem of producing appropriate calibration pieces for this type of work.

The detailed statistical analysis of the coating thickness data obtained shows the complexity of the task of developing standard techniques for these nonhomogeneous coatings and further shows that a great deal of further work is needed to formulate standards of calibration and measurements. The different methods were demonstrated to be reliable and reproducible, and all these already established nondestructive methods, when applied correctly, gave highly trustworthy results.

Table 9 Thickness values of the unknown samples: comparison between the average value of the round-robin test and data from destructive evaluation

	YPSZ-Armco A	YPSZ-Armco B	YPSZ-AISI 316 A	YPSZ-AISI 316 A
L, μm average of NDE	75 ± 18(a)	125 ± 50(a)	331 ± 42(a)	408 ± 37(a)
L, μm by DT	73 ± 30(a)	118 ± 24(a)	289 ± 30(a)	347 ± 30(a)
$\Delta L/L$, %	1.4	6	15	18

NDE, nondestructive evaluation; DT, destructive test. (a) The number after ± is the semiamplitude of thickness interval corresponding to a 95% probability of the *t*-student distribution.

Table 10 Thermal diffusivity reported for the coating material

Method	$\overline{\alpha}$ ($\times 10^{-4}$ m^2/s)	Participant No.
TWI (IR)	0.0065	3
TWI (PA)	0.0250 ± 0.03(a)	2
TWI (IR)	0.0050 ± 0.001	5
TWI (IR)	0.0057 ± 0.002	7
TWI (M)	0.0280 ± 0.002(a)	9
PPTR	0.0068 ± 0.004	6

TWI, thermal wave interferometry; IR, infrared radiometry; PA, photoacoustic; M, mirage; PPTR, pulsed photothermal radiometry. (a) Data refer to results that are outside the general trend for reasons explained in the text.

Acknowledgments

The editors are indebted to Dr. Paolo Fenici for supplying the working conditions and institutional support of this work. The editing services of MA Laura Keeler were greatly appreciated during the preparation of this manuscript.

The following working group is acknowledged.

D. Wu, W. Karpen, A. Salerno, and **G. Busse,** Institut für Kunststoffprüfung und Kunststoffkunde, Universität of Stuttgard, Pfaffenwaldring 32, D-70569 Stuttgard, Germany

U. Netzelmann, G. Walle, and **H. Zhang,** Fraunhofer-Institut für zerstörungsfreie Prüfverfahren (FhG-IzfP), University, Bldg. 37, D-66123, Saarbrücken, Germany

B.K. Bein, G. Kalus, J. Bolte, R. Hüttner, and **J. Pelzl,** AG Festkörperspektroskopie/ Solid State Spectroscopy, Exp. -Phys. III/ VI, Ruhr-Universität Bochum, D-44780 Bochum, Germany

M. Oksanen, R. Vuohelainen, and **M. Luukkala,** Department of Physics , University of Helsinki, P.O.Box 9, FIN-00014 University of Helsinki, Finland

D.P. Almond, School of Materials Science, University of Bath Claverotn Down, Bath BA2 7AY, UK

S.D. Preston, RD3/33 AEA Technology, Thermal Properties Laboratory, Risley, Warrington Cheshire, WA3 6AT, UK

L. Fabbri, M. Oksanen, F. Lakestani, H. Crutzen, and **P. Fenici,** European Union, Joint Research Centre, Institute for Advanced Materials, Ispra site, 21020 Ispra (VA) Italy

J.C. Krapez, F. Lepoutre, and **D.L. Balageas,** Division de Thermophysique, Office National D'Etudes et de Recherches Aérospatiales, POB 72, F-92322 Chatillon, France

M. Bertolotti, G.L. Liakhou, R. Li Voti, S. Paoloni, and **C. Siblia,** Dipartimento di Energetica, Universita' degli Studi di Roma "La Sapienza," Via Scarpa 16, 00141 Roma, Italy

References

1. D. Fournier and G.P. Roger, Ed., 8th International Topical Meeting on Photoacoustic and Photothermal Phenomena, *J. Phys. IV Coll. C7*, supplement *J. Phys. III*, (No. 7), Les Edition de Physique, Paris, 1994
2. D.P. Almond and P.M. Patel, Photothermal Science and Techniques, *Physics and Its Applied Series*, Vol 10, Chapman & Hall, 1996
3. P.C.A. Bennet, Jr. and R.R. Patty, Thermal Wave Interferometry: A Potential Application of the Photoacoustic Effect, *Appl. Optics*, Vol 21, 1982, p 49-54
4. D.P. Almond and P.M. Patel, Thermal-Wave Testing of Plasma-Sprayed Coatings and a Comparison of the Effects of Coating Microstructure on the Propagation of Thermal and Ultrasonic Waves, *J. Mater. Sci.*, Vol 20, 1985, p 955
5. B.K. Bein and J. Pelzl, Analysis of Surface Exposed to Plasmas by Nondestructive Photoacoustic and Photothermal Techniques, *Plasma Di-*

agnostics, Surf. Anal. Inter., A. Auciello and D.L. Flamm, Ed., Academic Press, 1989, p 211-326

6. J. Jaarinen, "Nondesructive Evaluation of Coatings by Low-Frequency Thermal Waves," Appl. Phys. Series No. 162, Academic Dissertation, Acta Polytecnica Scandinavica 1988 UDC 620.179.1
7. A.C. Bento and D.P. Almond, The Accuracy of Thermal Wave Interferometry for the Evaluation of Thermophysical Properties of Plasma-Sprayed Coatings, *Meas. Sci. Technol.*, Vol 6, 1995, p 10221027
8. B.K. Bein, J. Gibkes, J.H. Gu, R. Huttner, J. Pelzl, D.L. Balageas, and Déom, Thermal Wave Characterization of Plasma-Facing Materials by IR Radiometry, *J. Nucl. Mater.*, Vol 191-194, 1992, p 315-319
9. A.C. Tam and B. Sullivan, Remote Sensing Applications of Pulse Photothermal Radiometry, *Appl. Phys. Lett.*, Vol 43 (No. 4), 1983, p 333-335
10. A.C. Tam, Pulsed Photothermal Radiometry for Noncontact Spectroscopy, Material Testing and Inspection Measurements, *Infrared Phys.*, Vol 25 (No. 1/2), 1985, p 305-313
11. D.L. Balageas, J.C. Krapez, and P. Cielo, Pulsed Photothermal Modelling of Layered Materials, *J. Appl. Phys.*, Vol 59, 1986, p 348-357
12. J.C. Murphy, L.C. Aamodt, and G.C. Westel, Coating Thickness Determination Using Time Dependent Surface Temperature Measurements, *Review of Progress in Quantitative Nondestructive Evaluation*, Vol 6A, 1987), p 277-284
13. S.O. Kanstad and P.E. Nordal, Experimental Aspects of Photothermal Radiometry, *Can. J. Phys.*, Vol 64, 1986 p 1155
14. G. Busse, Photothermal Transmission Probing of a Metal, *Infrared Phys.*, Vol 20, 1979, p 419-422
15. L. Fabbri and P. Fenici, Three-Dimensional Photothermal Radiometry for the Determination of the Thermal Diffusivity of Solids, *Rev. Sci. Instrum.*, Vol 66, 1995, p 3593-3600
16. G. Busse, D. Wu, and W. Karpen, Thermal Wave Imaging with Phase Sensitive Modulated Thermography, *J. Appl. Phys.*, Vol 71 (No. 8), 1992, p 3962-3965
17. G. Busse, B. Bauer, W. Rippel, and D. Wu, Lockin Vibrothermal Inspection of Polymer Composites, Quantitative Infrared Thermography Proc., D. Balageas, G. Busse, and G.M. Carlomagno, Ed., Editions Européennes Thermique et Industrie, Paris, 1992, p 154-158
18. W.B. Jackson, N.M. Amer, A.C. Boccara, and D. Fournier, *Appl.Opt.*, Vol 20, 1981, p 1333
19. P.K. Kuo, E.D. Sendler, L.F. Favro, and R.L. Thomas, Mirage-Effect Measurement of Thermal Diffusivity, Part II: Theory, *Can. J. Phys.*, Vol 64, 1986, p 1168-1171
20. M. Bertolotti, R. Li Voti, G. Liakhou, and C. Sibilia, On the Photodeflection Method Applied to Low Diffusivity Measurements, *Rev. Sci. Instrum.*, Vol 64, 1993, p 1576
21. V. Thien, P. Vetterlein, M. Kröning, and E. Winschuh, Examination of Materials with the Mobile Thermal Microscope ALADIN, A New Analytical Tool of Materials Technology, *Mikrochim. Acta (Wien)*, Vol II, 1990, p 25-34
22. H.L. Libby, *Íntroduction to Electromagnetic Nondestructive Test Methods*, Robert E. Krieger Publishing Co., Inc., Malabar, Florida, 1971
23. D.H. Hasseman, L.F. Johnson, L.D. Bentsen, R. Syed, and H.L. Lee, *Am. Ceram. Soc. Bull.*, Vol 66, 1987, p 799-806
24. W.N. Lawless and T.K. Gupta, Thermal Properties of Tetragonal ZrO_2 at Low Temperature, *Phys. Rev. B*, Vol 28, 1983, p 5507-5510
25. J.R. Brandon and R. Taylor, Thermal Properties of Ceria and Yttria Partially Stabilized Zirconia Thermal Barrier Coatings, *Surf. Coat. Technol.*, Vol 34/40, 1989, p 143-151
26. Y.S. Touloukian, R.W. Powell, C.Y. Ho, and M.C. Nicoulaou, *Thermophysical Properties of Matter, Thermal Diffusivity*, Vol. 10, TPRC Data Services, IFI/Plenum, 1973
27. R.E. Taylor and K.D. Maglíc, *Compendium of Thermophysical Property Measurement Methods*, Vol 1, K.D. Maglíc, A. Cezairliyan, and V.E. Peletsky, Ed., Plenum, 1984
28. ANSI/ASTM C664-70: "Standard Test Method for Thickness of Diffusion Coatings, 1972 (Reapproved 1976), *1980 Annual Book of ASTM Standards, Part 17: Refractories, Glass, Ceramic Materials, Carbon, and Graphite Products*, ASTM, 1980, p 663
29. H. Crutzen, Ph.D. 1st year report, School of Industrial and Manufacturing Science, Cranfield University, Feb 1996
30. G. Grimvall, Thermophysical Properties of Materials, *Selected Topics in Solid State Physics*, Vol XVIII, North-Holland Physics Publishing, 1986
31. M. Bertolotti, V. Dorogan, G.L. Liakhou, R. Li Voti, S. Paoloni, and C. Sibilia, New Photothermal Deflection for Thermal Diffusivity Measurement of Semiconductor Wafers, *Rev. Sci. Instrum.*,Vol 64 (No. 1576), 1993, p 642-648
32. R. Brant, L. Pawlowsky, and G. Neuer, Specific Heat and Thermal Conductivity of Plasma Sprayed Yttria-Stabilized Zirconia and NiAl, NiCr, NiCrAl, NiCrAlY, NiCoCrAlY Coatings, *High Temp.-High Press.*, Vol 18, 1986, p 65-77